Figure S1

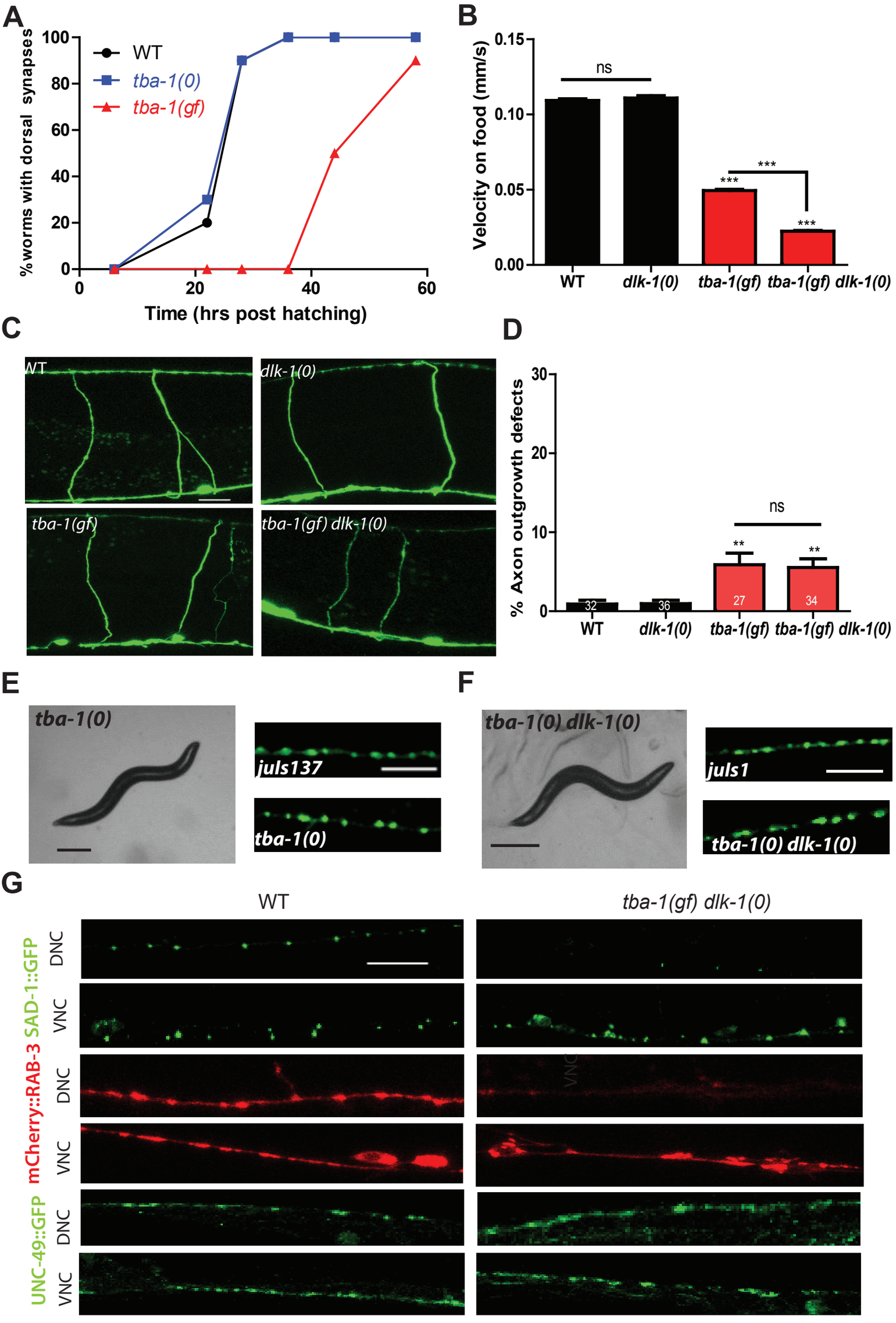
A
% worms with dorsal synapses
100
80
60
40
20
0
WT
tba-1(0)
tba-1(gf)
0
20
40
60
Time (hrs post hatching)
B
Velocity on food (mm/s)
0.15
0.10
0.05
0.00
ns
***
***
***
WT
dlk-1(0)
tba-1(gf)
tba-1(gf) dlk-1(0)
C
WT
dlk-1(0)
tba-1(gf)
tba-1(gf) dlk-1(0)
D
% Axon outgrowth defects
30
20
10
0
ns
**
**
32
36
27
34
WT
dlk-1(0)
tba-1(gf)
tba-1(gf) dlk-1(0)
E
tba-1(0)
juls137
tba-1(0)
F
tba-1(0) dlk-1(0)
juls1
tba-1(0) dlk-1(0)
G
WT
tba-1(gf) dlk-1(0)
SAD-1::GFP
DNC
VNC
mCherry::RAB-3
DNC
VNC
UNC-49::GFP
DNC
VNC

Figure S2

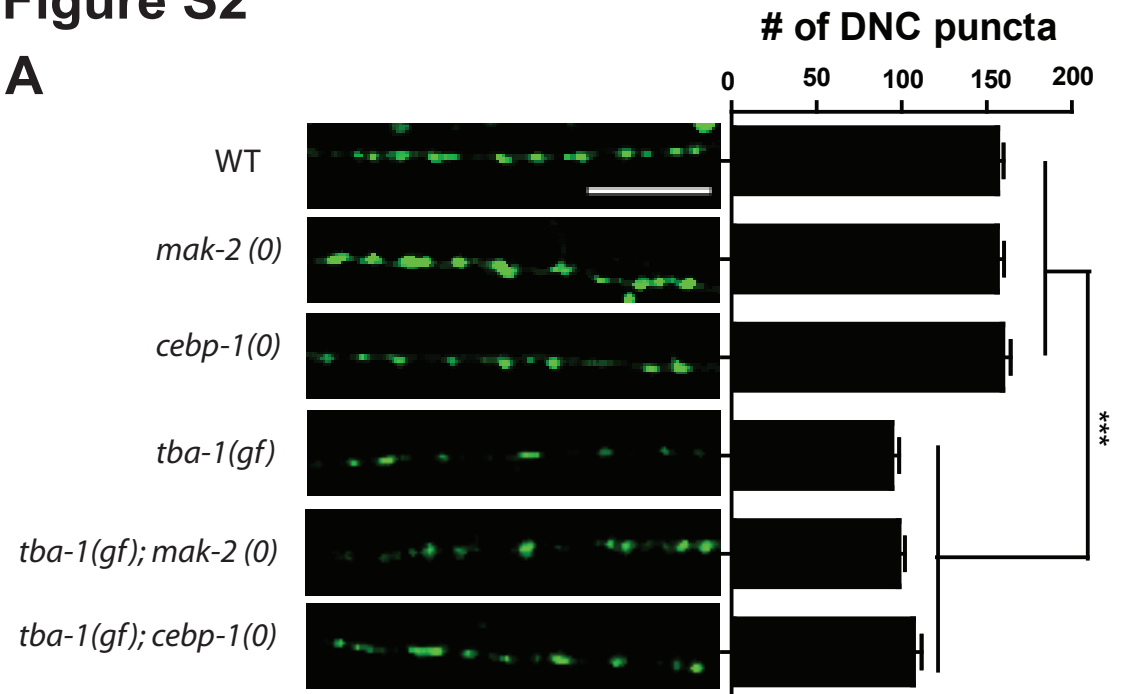
A
# of DNC puncta
0
50
100
150
200
WT
mak-2 (0)
cebp-1(0)
tba-1(gf)
tba-1(gf); mak-2 (0)
tba-1(gf); cebp-1(0)
***

Figure S3

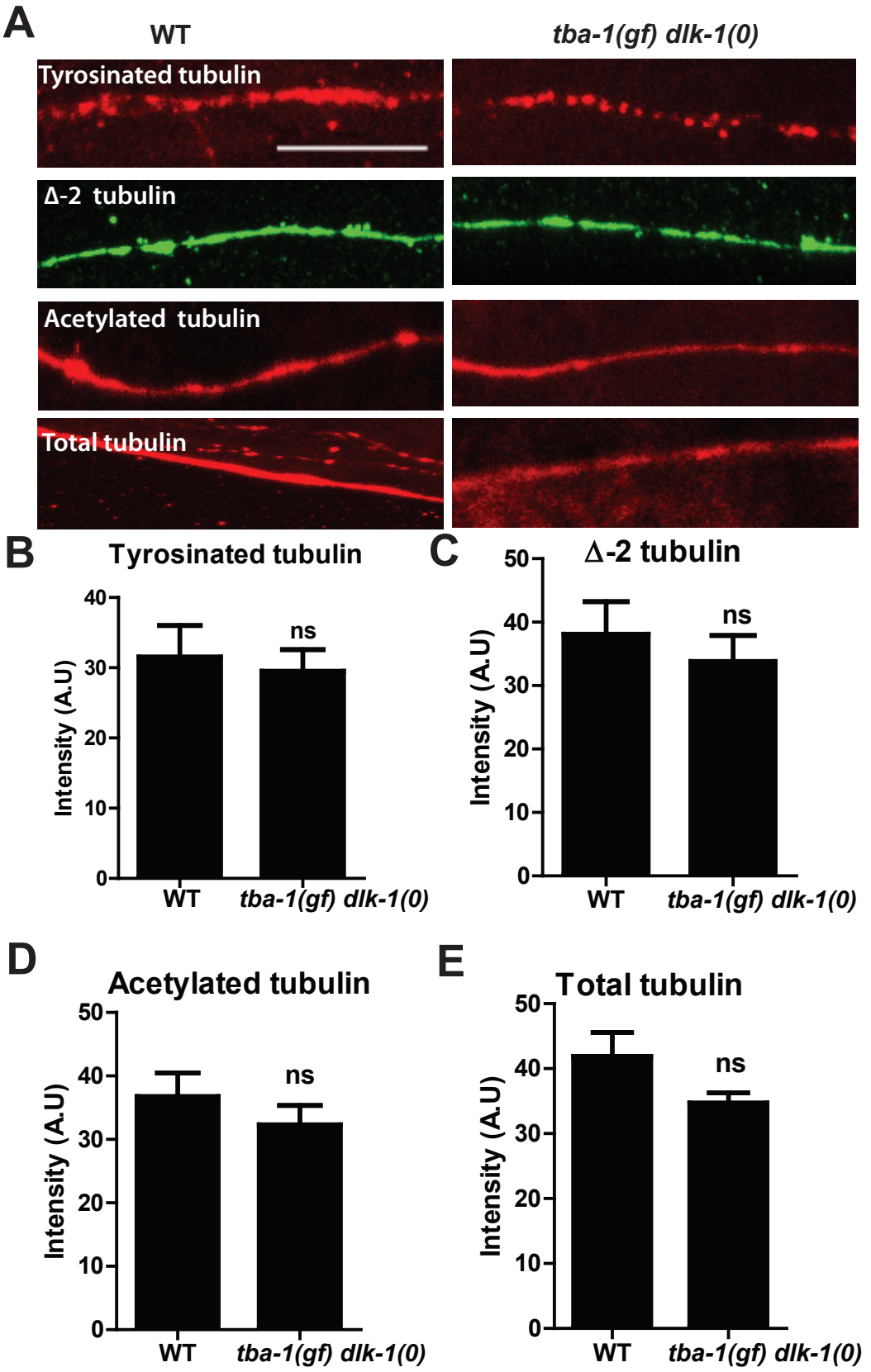
A
WT
tba-1(gf) dlk-1(0)
Tyrosinated tubulin
Δ-2 tubulin
Acetylated tubulin
Total tubulin
B
Tyrosinated tubulin
Intensity (A.U)
40
30
20
10
0
ns
WT
tba-1(gf) dlk-1(0)
C
Δ-2 tubulin
Intensity (A.U)
50
40
30
20
10
0
ns
WT
tba-1(gf) dlk-1(0)
D
Acetylated tubulin
Intensity (A.U)
50
40
30
20
10
0
ns
WT
tba-1(gf) dlk-1(0)
E
Total tubulin
Intensity (A.U)
50
40
30
20
10
0
ns
WT
tba-1(gf) dlk-1(0)

Figure S4

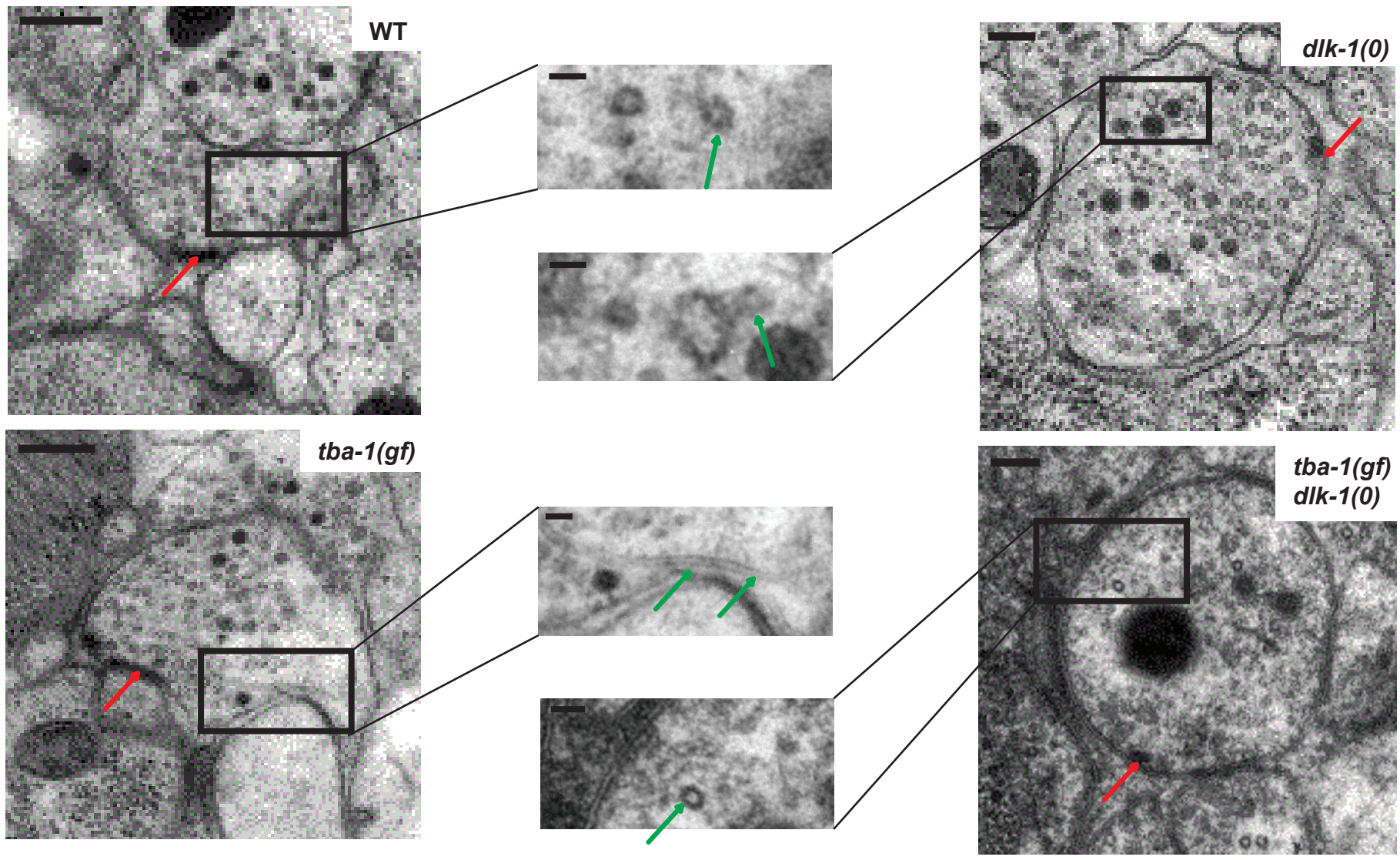
A
WT
dlk-1(0)
tba-1(gf)
tba-1(gf)
dlk-1(0)

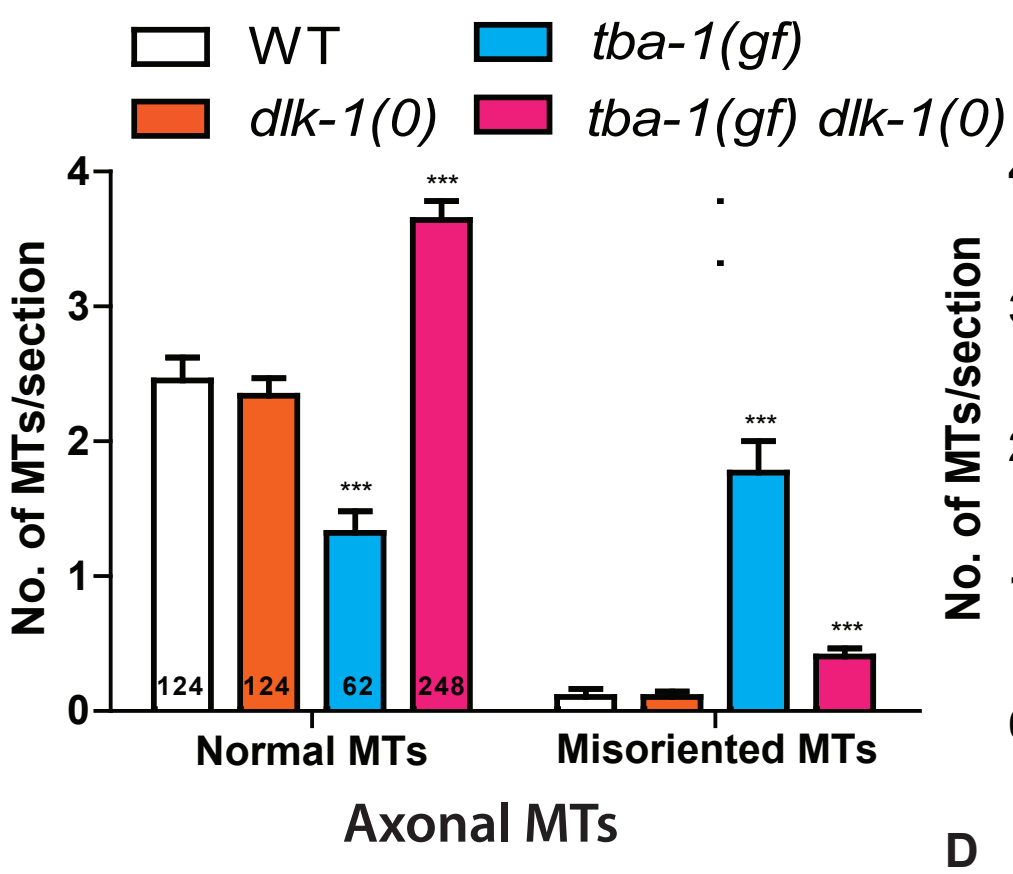
B
WT
dlk-1(0)
tba-1(gf)
tba-1(gf) dlk-1(0)
No. of MTs/section
Normal MTs
Misoriented MTs
Axonal MTs
124
124
62
248
***

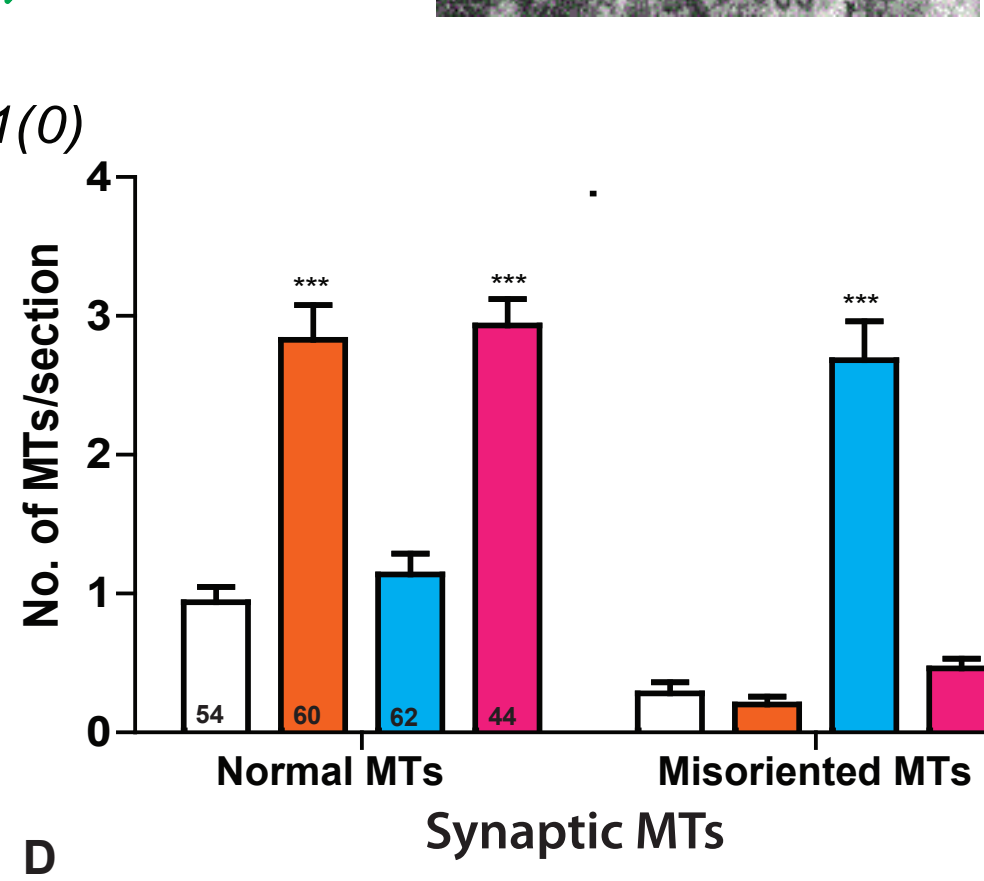
No. of MTs/section
Normal MTs
Misoriented MTs
Synaptic MTs
54
60
62
44
***

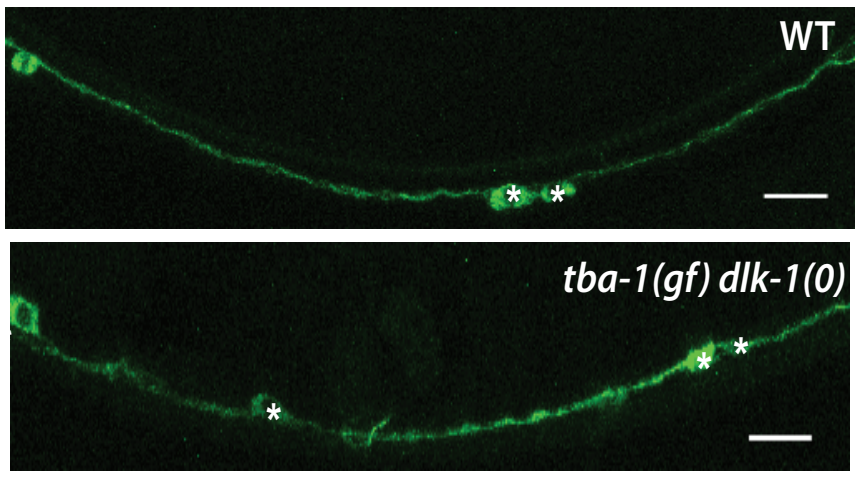
C
WT
tba-1(gf) dlk-1(0)

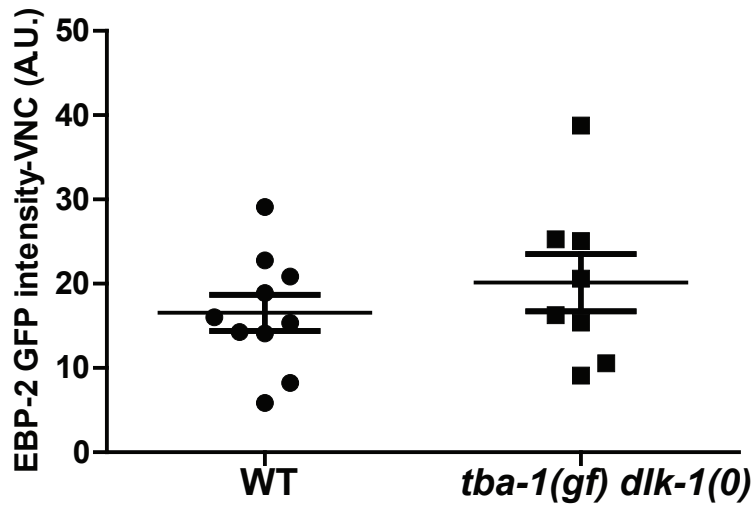
D
EBP-2 GFP intensity-VNC (A.U.)
WT
tba-1(gf) dlk-1(0)

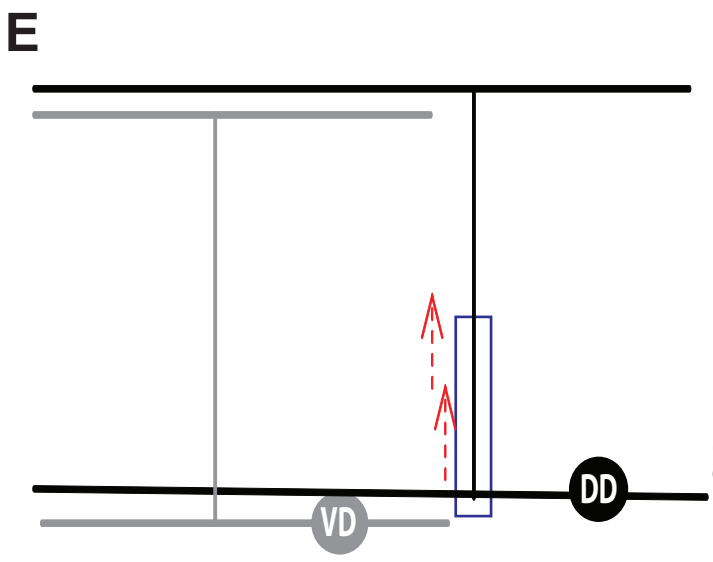
E
VD
DD

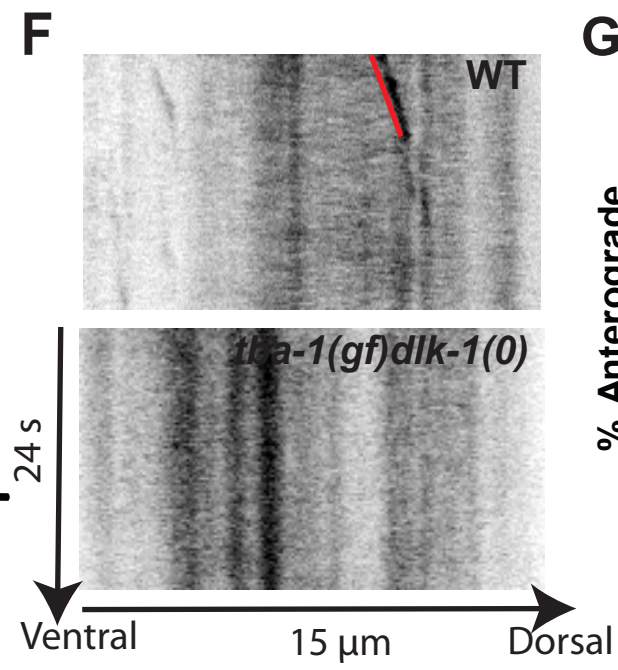
F
WT
tba-1(gf)dlk-1(0)
24 s
Ventral
15 µm
Dorsal

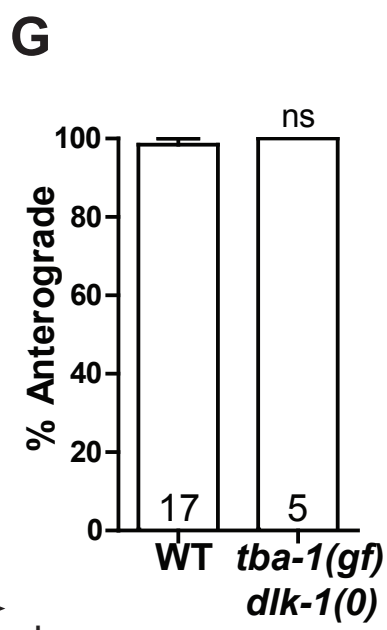
G
% Anterograde
ns
17
5
WT
tba-1(gf) dlk-1(0)

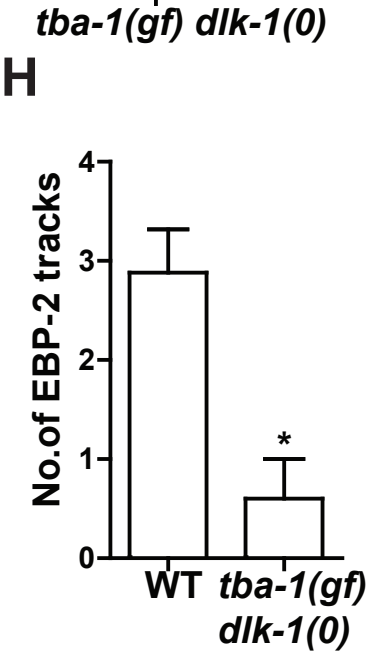
H
No.of EBP-2 tracks
*
WT
tba-1(gf) dlk-1(0)

Figure S5

A

ju972 (G274R)

```
H.s  GSEKVSKTGAEGAVLDEAKNINKSLSALGNVISALAEGTKTHVPYRDSKMTRILQDSLGG 294
M.m  GSEKVSKTGAEGAVLDEAKNINKSLSALGNVISALAEGTKTHVPYRDSKMTRILQDSLGG 294
D.m  GSEKVSKTGAEGTVLDEAKNINKSLSALGNVISALADGNKTHIPYRDSKLTRILQESLGG 300
C.e  GSEKVSKTGAQGTVLEEAKNINKSLTALGIVISALAEGTKSHVPYRDSKLTRILQESLGG 296
```

ju977 (E432K)

```
H.s  NIAPVVAGISTEEKEKYDEEISSLYRQLDDKDDEINQQSQLAEKLKQQMLDQDELLASTR 460
M.m  NITPVVDGISAE-KEKYDEEITSLYRQLDDKDDEINQQSQLAEKLKQQMLDQDELLASTR 459
D.m  ALANMSASVAVNEQARLATECERLYQQLDDKDEEINQQSQYAEQLKEQVMEQEELIANAR 480
C.e  MLTSTTGPITDEEKKKYEEERVKLYQQLDEKDDEIQKVSQELEKLRQQVLLQEEALGTMR 474
```

B

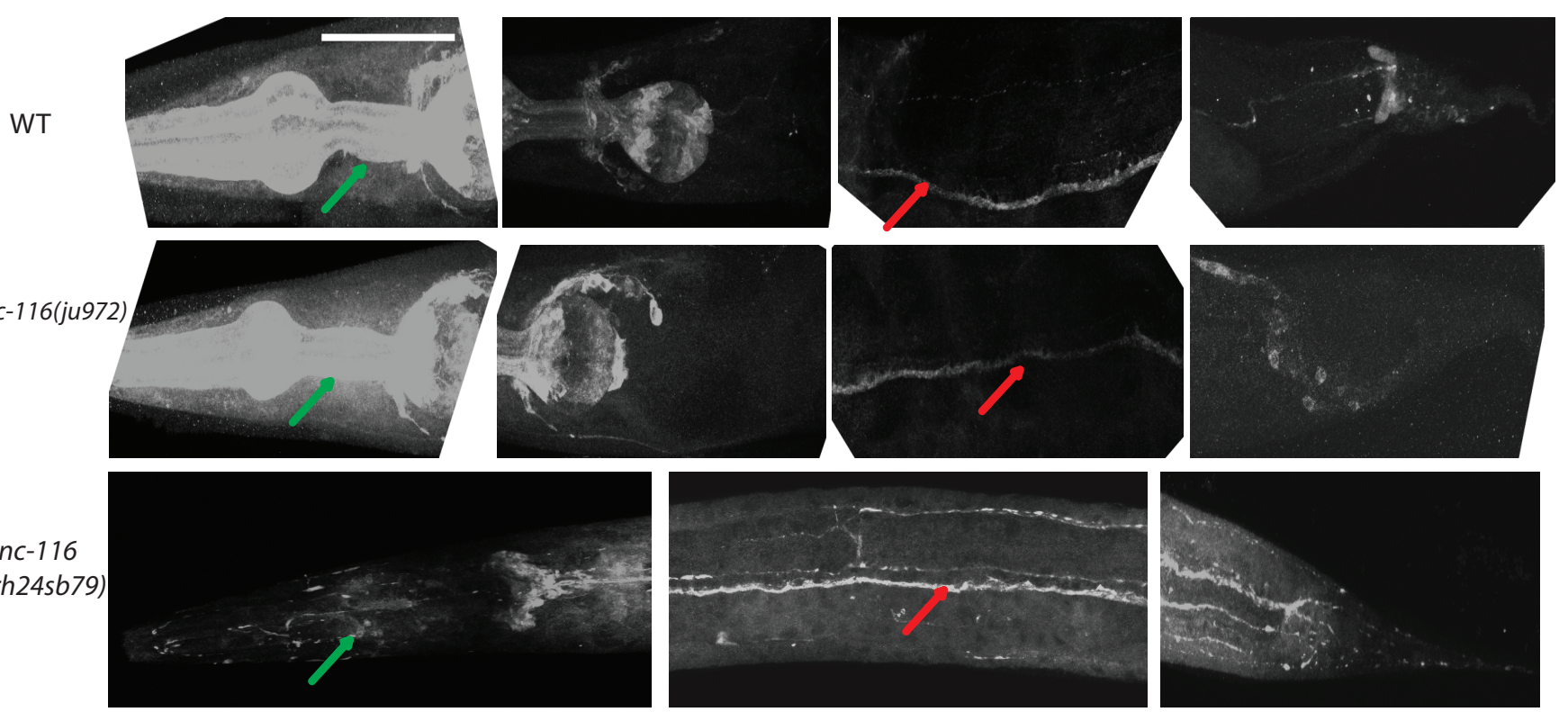

C

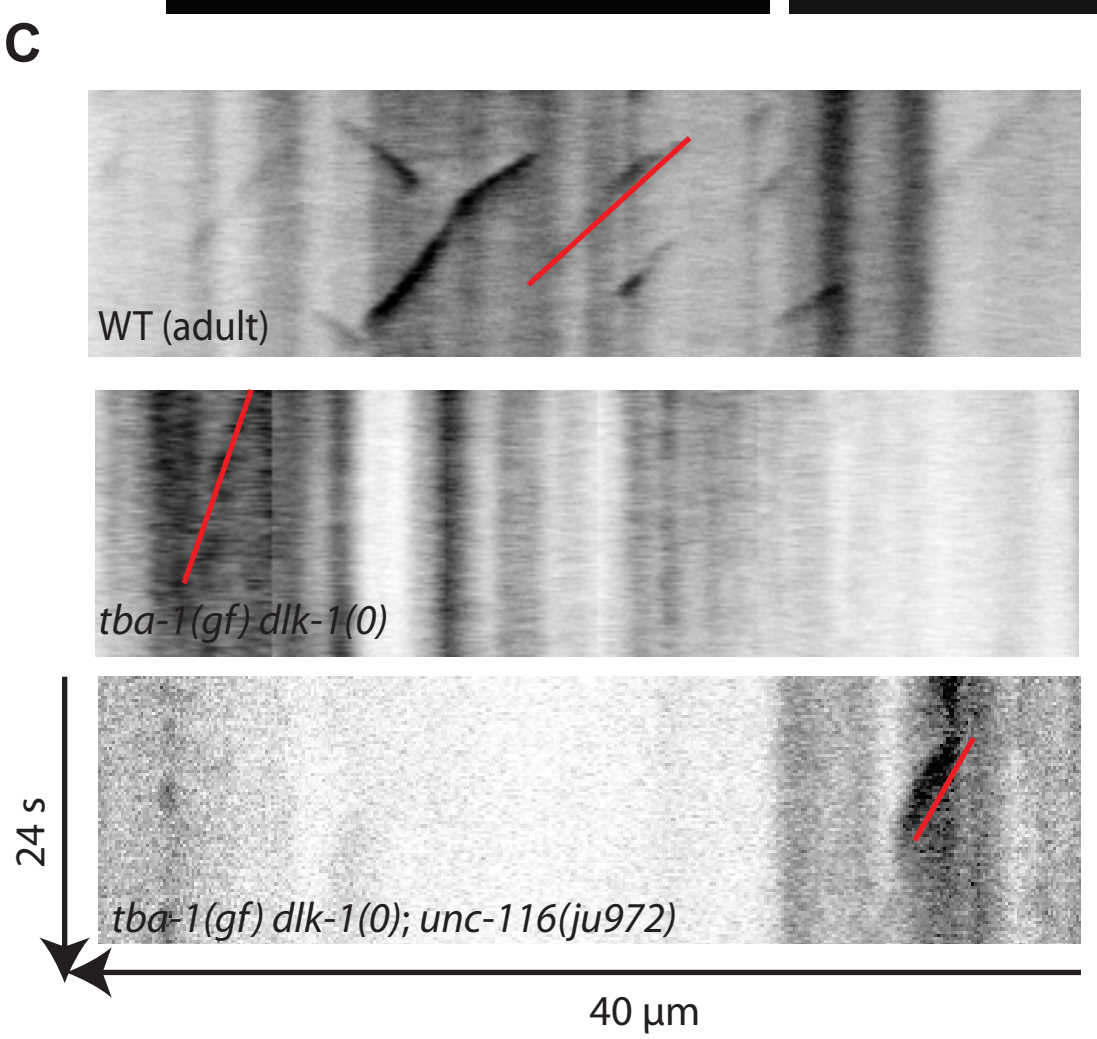

D

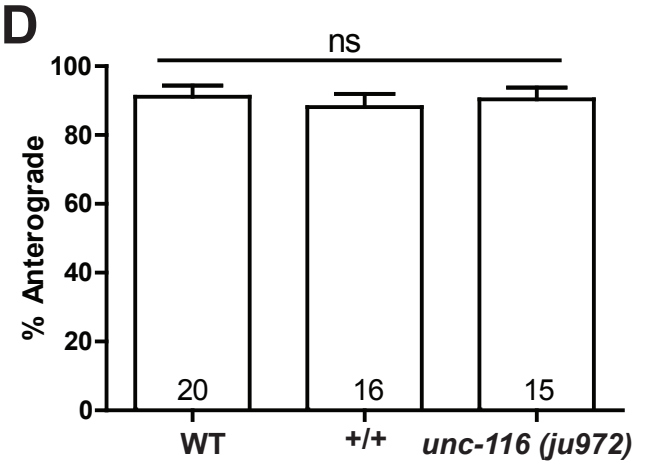

E

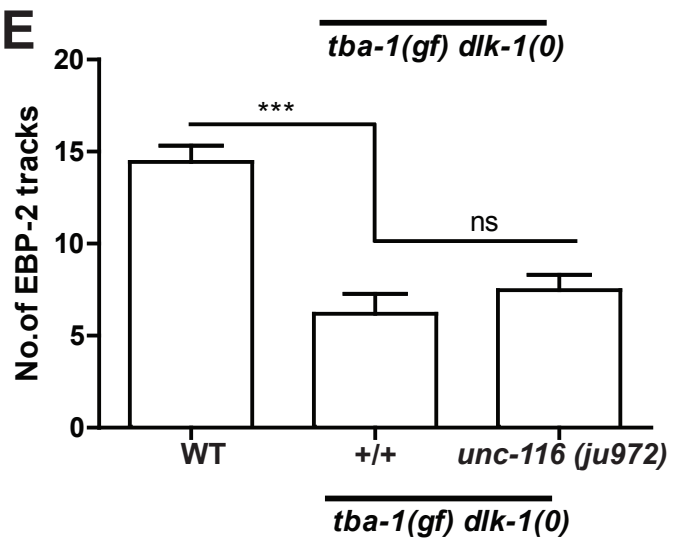

Supplementary Information

Supplementary Figure Legends

Figure S1 (related to Figure 1): (A) Remodeling time in WT, *tba-1(0)* and *tba-1(gf)* animals; n=10 animals per genotype per time point.

(B) Quantification of the locomotion velocity of WT, *dlk-1(0)*, *tba-1(gf)* and *tba-1(gf) dlk-1(0)* animals on food. Data are mean ± SEM; n=10 animals for each genotype. Statistics: One-way ANOVA followed by Tukey's posttest; ***p<0.001, ns-not significant.

(C) Images of axon morphology in WT, *dlk-1(0)*, *tba-1(gf)* and *tba-1(gf) dlk-1(0)* animals using P_{unc-25}-GFP (*juIs76*). Scale bar: 10 µm.

(D)Quantification of axon outgrowth defects (gaps in the axons and commissure branching defects) in WT, *dlk-1(0)*, *tba-1(gf)* and *tba-1(gf) dlk-1(0)* animals. Data are represented as mean ± SEM; n>27 animals per genotype. Statistics – One-way ANOVA followed by Tukey's posttest; **p<0.01, ns-not significant.

(E) Bright field image of a *tba-1(0)* animal, along with images of synapses in the dorsal cord of wild type and *tba-1(0)* using *juIs137* (P_{flp-13}-SNB-1::GFP). Scale bars- bright field: 200 µm and *juIs137*: 10 µm.

(F) Bright field image of a *tba-1(0) dlk-1(0)* animal, along with images of synapses in the dorsal cord of wild type and *tba-1(0) dlk-1(0)* using *juIs1* (P_{unc-25}-SNB-1::GFP). Scale bars- bright field: 200 µm and *juIs1*: 10 µm.

(G) Images of the DNC and VNC of WT and *tba-1(gf)dlk-1(0)* animals expressing P*unc-25* -SAD-1::GFP and P*unc-25* -mCherry::RAB-3 in the GABAergic D neurons, and UNC-49::GFP in body wall muscles . Scale bar: 10 µm.

Figure S2 (related to Figure 3): (A) (left) Images of DNC synapses of WT, *mak-2(0)*, *cebp-1(0)*, *tba-1(gf)*, *tba-1(gf); mak-2(0)* and *tba-1(gf); cebp-1(0)* adult animals using *juIs1* (P_{unc-25}-SNB-1::GFP). Scale bar: 10 µm. (right) Quantification of DNC synapses. ***p<0.001.

Figure S3 (related to Figure 4): (A) Representative images of tyrosinated tubulin, Δ-2 tubulin, acetylated tubulin and total tubulin immunostaining in the VNC of WT and *tba-1(gf) dlk-1(0)* animals. Scale bar: 10 µm.

(B-E) Quantification of (B) Tyrosinated, (C) Δ-2 tubulin, (D) Acetylated tubulin and (E) Total tubulin levels by immunostaining. Data are mean ± SEM; n=10 animals per genotype. Statistics – unpaired t-test; ns - not significant.

Figure S4 (related to Figure 4): (A) EM sections of synaptic boutons of DD neurons. Red arrowheads indicate active zones and green arrowheads indicate MTs. Scale bar (top left): 200 nm (main), 50 nm (enlarged).

(B, C) Quantification of the number of normal (perpendicular to the plane of the section) and misoriented (parallel to the plane of the section) MTs per section in the axonal (B) region and synaptic (C) region of the DD neuron. Data are represented as mean ± SEM; number of sections is indicated on each bar graph. Statistics- 2-Way ANOVA followed by Bonferroni posttest; ***p<0.001, when compared to WT.

(D) Images of EBP-2-GFP expression in the VNC of WT and *tba-1(gf) dlk-1(0)* animals. White asterisks on DD and VD cell bodies. Scale bar: 10 µm.

(E) Quantification of EBP-2::GFP intensity in the VNC of WT and *tba-1(gf) dlk-1(0)* animals. Statistics- unpaired t-test; data not significant.

(F) Schematic representation of EBP-2 tracks in the commissures of adult D neurons.

(G) Kymographs of adult WT and *tba-1(gf) dlk-1(0)* D neuron commissures.

(H, I) Quantification of (H) direction of movement and (I) number of EBP-2 tracks. Data are represented as mean ± SEM; number of animals for each genotype is represented on (H). Statistics: One-Way ANOVA followed by Tukey's posttest; *p<0.05, ns- not significant.

Figure S5 (related to Figure 6): (A) Alignment of UNC-116 protein in *C. elegans (C.e)*, *Drosophila (D.m)*, mouse (*M.m*) and human (*H.s*) homologs; G274R (green) - *ju972*, E432K (blue) - *ju977*.

(B) Images of wild type, *unc-116* animals (*ju972*, *rh24sb79*) stained using an antibody against the C-terminal of UNC-116. Green arrows point to pharyngeal staining and red arrows point to staining along the VNC. Scale bar: 50 µm

(C) Representative kymographs of EBP-2 movement in the adult VNC of WT, *tba-1(gf) dlk-1(0)* and *tba-1(gf) dlk-1(0); unc-116(gf)* animals.

(D, E) Quantification of (D) direction of movement and (E) number of EBP-2 tracks in WT, *tba-1(gf) dlk-1(0)* and *tba-1(gf) dlk-1(0); unc-116(ju972)* adults. Data are mean ± SEM; number of animals is depicted on (c). Statistics- One way ANOVA followed by Tukey's posttest; ***p<0.001, ns-not significant.

Supplementary Experimental Procedures

Isolation of *unc-116(ju972)* and *unc-116(ju977)*

tba-1(gf) dlk-1(0) animals were mutagenized using Ethyl Methane Sulphonate (EMS) following standard procedures [S1]. F2 animals with improved locomotion were selected as putative suppressors in a non-clonal screen. Several suppressors were determined to be intragenic loss of function mutations in *tba-1(gf)* and contained either stop codon changes or missense mutations (not shown). *ju972* and *ju977* were determined to be extragenic and mapped to the gene *unc-116* following whole genome sequence analysis by MAQGene [S2].

Strain construction

C. elegans strains were grown at 20^{o}C on NGM plates, following standard procedures [S1]. All compound mutants were verified using PCR based genotyping. The genotypes of all the strains used in the study are listed below.

Strain	Genotype	Allele or Transgene
CZ333	*juIs1 IV*	*juIs1* [*Punc-25-SNB-1::GFP; lin-15(+)*] [S3]
CZ2569	*tba-1(ju89) I; juIs1 IV*	*ju89*: Gly414Arg (C1581T) [S4]
CZ2060	*juIs137 II*	*juIs137* [*Pflp-13-$_{SNB}$-1::GFP; lin-*

		15(+)] [S5]
CZ18652	*dlk-1(tm4024) I; juIs137 II*	
CZ2411	*tba-1(ju89) I; juIs137 II*	
CZ16989	*tba-1(ju89)dlk-1(tm4024) I; juIs137 II*	
CZ4152	*juIs76 II*	*juIs76* [*Punc-25-GFP; lin-15(+)*] [S6]
CZ15941	*dlk-1(tm4024) I; juIs76 II*	
CZ14295	*tba-1(ju89) I; juIs76 II; juIs231*	*juIs231* [*Punc-25-mCherry::RAB-3; Pttx-3-RFP*] [S4]
CZ16587	*tba-1(ju89)dlk-1(tm4024) I; juIs76 II*	
CZ20317	*tba-1(ok1135)I; juIs137 II*	*ok1135*: 1 kb deletion [S7]
CZ13936	*hpIs1 II; juIs231*	*hpIs1* [*Punc-25-SAD-1::GFP(L,S); lin-15(+)*] [S8]
CZ14300	*tba-1(ju89)dlk-1(tm4024) I; hpIs1 II; juIs231*	
CZ21581	*juIs137 II; juEx6537*	*juEx6537* [*Punc-25-TBA-1; Pttx-3-GFP*]
CZ21584	*tba-1(ju89)dlk-1(tm4024) I; juIs137 II; juEx6537*	
CZ21587	*juIs137 II; juEx6540*	*juEx6540* [*Punc-25-DLK-1(minigene); Pttx-3-GFP*]
CZ21590	*tba-1(ju89)dlk-1(tm4024) I; juIs137 II; juEx6540*	
CZ3505	*juIs137 II; pmk-3(ok169) IV*	*ok169*: 1272bp deletion [S7]
CZ20316	*tba-1(ju89) I; juIs137 II; pmk-3(ok169) IV*	
CZ21574	*juIs1IV; cebp-1(tm2807)X*	*tm2807*: 479bp deletion [S7]
CZ15863	*tba-1(ju89)I; juIs1IV; cebp-1(tm2807)X*	
CZ8763	*mak-2(ok2394)juIs1IV*	*ok2394*: 878bp deletion [S7]
CZ19779	*tba-1(ju89)I; mak-2(ok2394)juIs1IV*	
CZ20219	*juIs137II; spas-1(ok1608)V*	*ok1608*:627bp deletion [S7
CZ22154	*tba-1(ju89)I; juIs137II; spas-1(ok1608)V*	
CZ19774	*juIs137 II; oxEx1268*	*oxEx1268* [*Phsp-16.2-DLK-1::mCherry; Pmyo-2-GFP*] [S9]
CZ19775	*tba-1(ju89)dlk-1(tm4024) I; juIs137 II; oxEx1268*	
CZ20215	*tba-1(ju89) I*	
CZ15956	*dlk-1(tm4024) I*	
CZ16631	*tba-1(ju89)dlk-1(tm4024) I*	
CZ17824	*juEx5317*	*juEx5317* [*Punc-25-EBP-2::GFP; Pgcy-8-GFP*]
CZ20216	*dlk-1(tm4024) I; juEx5317*	
CZ20217	*tba-1(ju89) I; juEx5317*	
CZ20218	*tba-1(ju89)dlk-1(tm4024) I; juEx5317*	
CZ20615	*oxIs22*	*oxIs22* [*Punc-49::UNC-49-B::GFP; lin-15(+)*] [S10]
CZ18274	*tba-1(ju89)dlk-1(tm4024) I; oxIs22*	
CZ21928	*juIs137 II; klp-7(tm2143) III*	*tm2143*:875bp deletion [S7]
CZ21575	*tba-1(ju89) I; juIs137 II; klp-7(tm2143) III*	
CZ16994	*tba-1(ju89)dlk-1(tm4024) I;unc-116(ju972) III; juIs1 IV*	*ju972*: Gly274Arg (G1400A)
CZ16992	*tba-1(ju89)dlk-1(tm4024) I;unc-*	*ju977*: Glu432Lys (G1921A)

	116(ju977) III; juIs1 IV	
CZ16634	*unc-116(ju977) III; juIs1 IV*	
CZ16629	*tba-1(ju89) I; unc-116(ju977) III; juIs1 IV*	
CZ16633	*unc-116(ju972) III; juIs1 IV*	
CZ16991	*tba-1(ju89) I; unc-116(ju972) III; juIs1 IV*	
CZ17360	*dlk-1(tm4024) I; unc-116(ju972) III; juIs1 IV*	
CZ4819	*unc-104(e1265) II; juIs1 IV*	*e1265*:Asp1541Asn (G4489A) [S7]
CZ21577	*unc-104(e1265) II; unc-116(ju972) III; juIs1 IV*	
CZ22740	*unc-104(e1265) II; unc-116(ju977) III; juIs1 IV*	
CZ21578	*tba-1(ju89)dlk-1(tm4024) I; unc-116(ju972) III; juEx5317*	
HR527	*unc-116(rh24sb79) III*	*rh24*: Ile302Met and Glu338Lys *sb79*: Gly45Glu [S11]
CZ17826	*juIs1 IV; juEx5319*	*juEx5319* [*Punc-116-UNC-116(ju972); Pmyo-2-mCherry*]
CZ18277	*tba-1(ju89)dlk-1(tm4024) I; juIs1 IV; juEx5459*	*juEx5459* [*Punc-116-UNC-116(ju977); Pgcy-8-GFP*]
CZ18280	*tba-1(ju89)dlk-1(tm4024) I; juIs1 IV; juEx5462*	*juEx5462* [*Punc-116-UNC-116(ju972); Pgcy-8-GFP*]
CZ19771	*tba-1(ju89)dlk-1(tm4024) I; juIs1 IV; juEx5992*	*juEx5992* [*Prgef-1-UNC-116(E273A); Pgcy-8-GFP*]
CZ20319	*tba-1(ju89)dlk-1(tm4024) I; unc-116(ju972) III; juIs1 IV; juEx6179*	*juEx6179* [*Fosmid-WRM06276D08; Pgcy-8-GFP*]
CZ20322	*tba-1(ju89)dlk-1(tm4024) I; unc-116(ju977) III; juis1 IV; juEx6182*	*juEx6182* [*Fosmid-WRM06276D08; Pgcy-8-GFP*]
CZ21925	*tba-1(ju89)dlk-1(tm4024) I;unc-116(ju972) III; juIs1 IV; juEx6624*	*juEx6624* [*Prgef-UNC-116; Pgcy-8-GFP*]

Plasmid and transgene generation

Plasmids were generated using Gateway technology (Invitrogen). Genomic DNA for *unc-116* and *tba-1* were amplified from purified genomic DNA by PCR using Phusion HF DNA polymerase (Finnzyme), and subcloned into PCR8 entry vectors. Site-directed mutagenesis was performed using Pfu Ultra polymerase (Agilent Technologies) to generate mutations corresponding to UNC-116(G274R), UNC-116(E432K) and UNC-116(E273A) following manufacturer protocols. The *dlk-1* minigene contained cDNA from exon 1-6 and exon 8 onwards, and genomic DNA in exon 6-8, as previously described [S12]. Primer and sequence information is available on request for all the clones generated in this study. Transgenic animals were generated by microinjection, following standard procedures [S13], using plasmids of interest at 1-5 ng/ul and Pgcy-8-GFP or Pttx-3-GFP (80-90 ng/ul) as co-injection markers. A minimum of 2-3 transgenes were generated for each construct described in this study. For rescue experiments using *unc-116*, *tba-1* and *dlk-1* constructs, the data from 3 transgenes was pooled in statistical analyses. The plasmids injected to make the transgenic lines used in this study are listed below.

Plasmid	Description	Transgenes generated
pCZGY2332	Punc-25 (2kb promoter)-EBP-2 cDNA-mGFP-unc-54 3'UTR	*juEx5317, juEx5318*
pCZGY2626	Punc-116 (2kb promoter)-unc-116 genomic DNA with G274R-unc-54 3'UTR	*juEx5319, juEx5462-5464*
pCZGY2627	Punc-116 (2kb promoter)-unc-116 genomic DNA with E432K-unc-54 3'UTR	*juEx5640-5642*
pCZGY2628	Punc-25 (2kb promoter)-dlk-1 minigene-unc-54 3'UTR [S10]	*juEx6540-6542*
pCZGY2630	Punc-25 (2kb promoter)-tba-1 genomic DNA-unc-54 3'UTR	*juEx6537-6539*
pCZGY2633	Prgef-1 (3.5kb promoter)-unc-116 genomic DNA-unc-54 3'UTR	*juEx6624-6626*
pCZGY2634	Prgef-1 (3.5kb promoter)-unc-116 genomic DNA with E273A-unc-54 3'UTR	*juEx5992-5994*

Antibodies and immunostaining

The primary antibodies used were mouse monoclonal DM1A for α-tubulin (Sigma) at 1:400 dilution, mouse monoclonal α-6B11-1 for acetylated tubulin (Sigma) at 1:500 dilution, rabbit polyclonal anti-Δ2-tubulin (Millipore AB3203) at 1:500 dilution, monoclonal rat anti-tyrosinated tubulin YL1/2 (Santa Cruz Biotechnology) at 1:100 dilution and polyclonal rabbit anti-UNC-116 antibody at 1:500 dilution [S14]. Alexa conjugated secondary antibodies were from Molecular Probes, and used at 1: 2,000 dilutions. Whole mount immunostaining was performed following the Finney and Ruvkun protocol [S15] with minor modification. Briefly, worms of mixed stages were fixed in 1% paraformaldehyde and repeated freeze-thaw cycles with liquid N_2. Samples were then treated with 1% β-mercaptoethanol and DTT to break the disulfide links in the cuticle, after which they were incubated with primary and secondary antibodies. Confocal images of the VNC about 50 µm posterior to the vulva were quantified.

Heat shock induced expression of *dlk-1*

Transgenic animals expressing *oxEx1268* (*$P_{hsp\text{-}16.2}$DLK-1-mCherry; $P_{myo\text{-}2}$GFP*) [S9] in the wild type and *tba-1(gf) dlk-1(0)* backgrounds were selected by positive pharyngeal GFP expression. L1, L2, L3, L4 and young adult animals were heat shocked at 33°C for 2 hours in an incubator. Heat shocked animals were maintained at 20°C after heat shock until they reached day 1 adulthood, when they were imaged using a Zeiss LSM 710 confocal microscope.

EBP-2::GFP image acquisition and analysis

Animals were anaesthetized in 0.6 mM levamisole on 2% agar pads for image acquisition. Live imaging for monitoring EBP-2 dynamics was done using a Yokogawa CSU-X1 spinning disc confocal head with a Photometrics Cascade II EMCCD camera (1,024 X 1,024 active pixels) controlled by µManager (http://www.micro-manager.org). 100 single plane images were taken serially at an exposure time of 114ms with an interval of 230ms between each frame, and analyzed using Metamorph software (Molecular Devices) to generate kymographs for analysis.

Modeling the motor head of UNC-116

The UNC-116 motor head shares 80% sequence identity with residues 254-341 of rat kinesin-1(Kif5c Nkhc2) and 75% identity with residues 8-358 *Drosophila* kinesin-1 (Khc kin CG7765). Using the solved crystal structure of rat (PDB ID: 2kinB) and *Drosophila* (PDB ID: 2y65C) kinesin-1 [S16, S17], the structure of UNC-116 was modeled using SWISS-Model (http://swissmodel.expasy.org/) and viewed using PyMOL (The PyMOL Molecular Graphics System, Version 1.3.0.4 Schrödinger, LLC).

EM serial reconstruction

Animals of the desired developmental stage (L1 or one-day old adults) were immobilized using high-pressure fixation with a high-pressure freezer (BAL-TEC HPM 010) at -176°C [S18]. The samples were freeze substituted in 2% osmium tetroxide and 0.1% uranyl acetate in acetone at -90°C (48 hrs) and then at -20°C (16 hrs) using a freeze-substitution apparatus (Leica EM AFS2). After infiltration and embedding in Durcupan ACM resin blocks, the samples were polymerized at 60°C for 48 hrs. Serial sections of 50 nm thickness were collected from the anterior part of the worm (after the posterior pharyngeal bulb) using Leica ULTRACUT UCT. Sections were collected onto pioloform coated slot grids and were stained for 5 minutes in 2.5% uranyl acetate in 70% methanol, followed by washing in Reynold's lead citrate for 3 minutes. Serial images from both the dorsal and ventral nerve cords were collected with a Gatan digital camera with 2,688 X 2,672 pixel resolution (using Gatan Digital Micrograph acquisition software) on a transmission electron microscope (JEOL-1200 EX, 80kv) at 10,000× magnification. Digital images from both nerve cords were then imported into Reconstruct 3D reconstruction software. Sections were realigned for accurate 3D measurements and visualization. Membranes, synaptic densities, vesicles and microtubules were manually traced on the serial image sections with Wacom Graphire3 Pen Tablet input hardware. The 3D scenes were rendered and saved as a 360° bitmap images.

References:

S1. Brenner, S. (1974). The genetics of *Caenorhabditis elegans. Genetics, 77*, 71–94.

S2. Bigelow, H., Doitsidou, M., Sarin, S., & Hobert, O. (2009). MAQGene: software to facilitate *C. elegans* mutant genome sequence analysis. *Nature methods*, *6*, 549.

S3. Hallam, S.J. & Jin, Y. (1998) *lin-14* regulates the timing of synaptic remodeling in *Caenorhabditis elegans*. *Nature*, *395*, 644-647.

S4. Baran, R., Castelblanco, L., Tang, G., Shapiro, I., Goncharov, A., & Jin, Y. (2010). Motor neuron synapse and axon defects in a *C. elegans* alpha-tubulin mutant. *PloS one*, *5*: e9655.

S5. Sakaguchi-Nakashima, A., Meir, J. Y., Jin, Y., Matsumoto, K., & Hisamoto, N. (2007). LRK-1, a *C. elegans* PARK8-related kinase, regulates axonal-dendritic polarity of SV proteins. *Current biology*, *17*, 592-8.

S6. Huang, X., Cheng, H.J, Tessier-lavigne, M., & Jin, Y. (2002). MAX-1, a Novel PH / MyTH4 / FERM domain cytoplasmic protein implicated in netrin- mediated axon repulsion. *Neuron*, *34*, 563-576.

S7. http://www.wormbase.org/

S8. Kim, J. S. M., Hung, W., Narbonne, P., Roy, R., & Zhen, M. (2010).*C. elegans* STRAD α and SAD cooperatively regulate neuronal polarity and synaptic organization. *Development*, *102*, 93-102.

S9. Hammarlund, M., Nix, P., Hauth, L., Jorgensen, E.M., & Bastiani, M. (2009). Axon Regeneration requires a conserved MAP Kinase Pathway. *Science*, *323*, 802-806.

S10. Bamber, B. A., Beg, A. A., Twyman, R. E., & Jorgensen, E. M. (1999). The *Caenorhabditis elegans unc-49* locus encodes multiple subunits of a hetero-multimeric GABA Receptor. *J. Neurosci.*, *19*, 5348-5359.

S11. Yang, H.Y., Mains, P. E., & McNally, F. J. (2005). Kinesin-1 mediates translocation of the meiotic spindle to the oocyte cortex through KCA-1, a novel cargo adapter. *JCB*, *169*, 447-57.

S12. Yan, D., & Jin, Y. (2012). Regulation of DLK-1 kinase activity by calcium-mediated dissociation from an inhibitory isoform. *Neuron*, *76*, 534-48.

S13. Mello, C. C., Kramer, J. M., Stinchcomb, D., & Ambros, V. (1991). Efficient gene transfer in *C. elegans*: extrachromosomal maintenance and integration of transforming sequences. *The EMBO Journal*, *10*, 3959-3970.

S14. McNally, K.L., Martin, J.L., Ellefson, M., and McNally, F.J. (2010). Kinesin dependent transport results in polarized migration of the nucleus in oocytes and inward movement of yolk granules in meiotic embryos. *Dev. Biol., 339,*126–140.

S15. Finney, M., & Ruvkun, G. (1990). The *unc-86* gene product couples cell lineage and cell identity in *C. elegans*. *Cell*, *63*, 895-905.

S16. Kozielski, F., Sack, S., Marx, A., Thormahlen, M., Schonbrunn, E., Biou, V., Thompson, A., Mandelkow, E.M. & Mandelkow, E. (1997). The crystal structure of dimeric kinesin and implications for microtubule-dependent motility. *Cell*, *91*, 985-994.

S17. Yi, H., Kaan, K., Hackney, D. D., & Kozielski, F. (2011). The structure of the kinesin-1 motor-tail complex reveals the mechanism of autoinhibition. *Science*, *333*, 883-5.

S18. Rostaing, P., Weimer, R. M., Jorgensen, E. M., & Triller, A. (2004). Preservation of immunoreactivity and fine structure of adult *C. elegans* tissues using high-pressure freezing. *Journal of Histochemistry & Cytochemistry*, *52*, 1-12.